THIRD EUROPEAN ROTORCRAFT AND POWERED LIFT AIRCRAFT FORUM

Paper No. 43

CALCULATION OF THE VISCOUS FLOW AROUND HELICOPTER BODIES

R. STRICKER

G. POLZ

MESSERSCHMITT-BÖLKOW-BLOHM GMBH

MUNICH, GERMANY

September 7-9, 1977

AIX-EN-PROVENCE, FRANCE

ASSOCIATION AERONAUTIQUE ET ASTRONAUTIQUE DE FRANCE

CALCULATION OF THE VISCOUS FLOW AROUND HELICOPTER BODIES [1]

R. Stricker, G. Polz
Messerschmitt-Bölkow-Blohm GmbH
Munich, Germany
P.O.Box 801140

Summary

To reduce expensive wind tunnel tests, analytical techniques for helicopter fuselage design and optimization, useful for preliminary design studies of new helicopters, become of increasing importance. As a tool for fuselage design, a method for calculation of the flow field around helicopter bodies is presented, including viscous and separation effects.

A potential flow model for the iterative calculation of separated flow around blunt bodies is developed:
First velocities around the body are calculated by a potential flow panel method, neglecting skin friction and separated flow when running the first iteration loop. A set of streamlines on the body surface is then determined using two-dimensional spline interpolation for velocities and geometry. Separation line on the body surface is found by a quasi-two-dimensional boundary layer calculation. To simulate the wake, a wake body with a continuous vorticity distribution is attached to the body at the separation line. The wake body surface is formed by streamlines and the vorticity is defined by the velocity profiles at the separation line. Potential flow around the body and in the wake is recalculated taking into consideration the wake influence.

Theoretical results are shown for a sphere and a helicopter fuselage:
At the sphere the separated flow region agrees well with measurements and the calculated wake shows typical properties of separated flow such as the wake contraction, the finite reverse flow area, and the characteristic velocity profiles.
Calculations of flow fields around a helicopter body demonstrate the effectiveness of the method in estimating the separated flow area and the wake geometry for a helicopter configuration, so that forces and moments acting on the fuselage as well as wake-tail interference effects can be calculated.

[1] Work sponsored by the Ministry of Defence of the Federal Republic of Germany

Notations

A	coefficient matrix
a	constant, wake cross section area
B	right hand side vector
C	body influence coefficient
c	constant
D	wake influence coefficient
e	unity vector
n	normal vector
p	point of reference
RE	Reynolds number
r	distance
s	surface of the body
t	streamline coordinate
u	velocity
v	volume of the wake
x, y, z	rectangular coordinates
Γ	circulation
σ	source distribution
ψ	stream function
ω	vorticity distribution
∇	nabla operator

Indices

p	point of reference
sl	separation line
T	transformed
w	wake
σ	source distribution
ω	vorticity distribution
∞	infinity
$\rightarrow$	vector

1. Introduction

The shape of a helicopter body in general is a compromise of non-aerodynamic and aerodynamic requirements, which are contrary to some extent. Depending on the mission of the helicopter the non-aerodynamic or the aerodynamic requirements dominate: I.e. the shape of a crane helicopter working in the low speed region is mostly influenced by non-aerodynamic requirements, whereas a utility helicopter shows an airframe designed to meet also some aerodynamic requirements.

Typical non-aerodynamic requirements are the size of passenger/freight cabin, the location of necessary components (such as power plant, gear box, tail rotor, weapons and external loads), and some other criteria such as easy access, rear door, ground clearence and visibility.

The main aerodynamic requirement is the reduction of helicopter parasite drag to get good cruising speed and fuel economy. According to Figure 1 the multi purpose helicopter BO 105, e.g.,

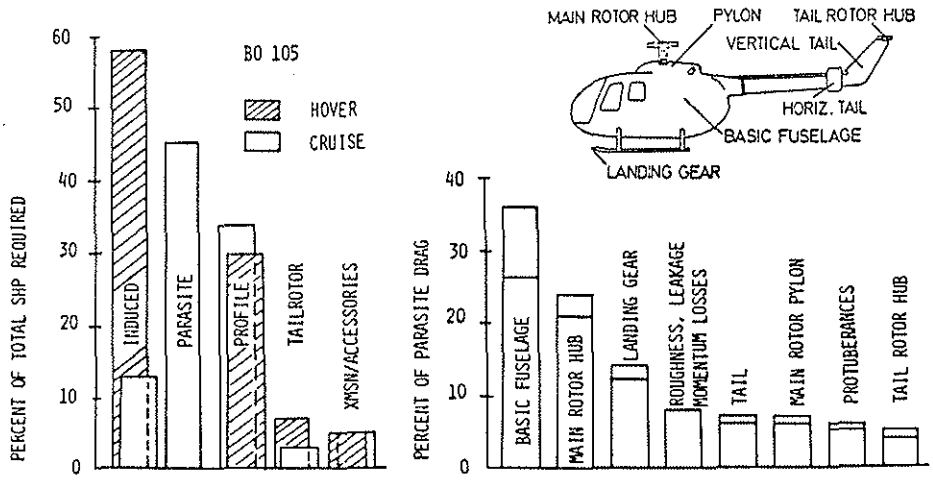

Figure 1 Breakdown of Power Required and of Parasite Drag for a Typical Utility Helicopter

requires about 45 percent of the total power to overcome the parasite drag at cruising speed. Main sources of parasite drag are the basic fuselage, the rotor hub, the landing gear, the rotor pylon and the tail, Reference 1. But also flight mechanic parameters are affected by the aerodynamic characteristics of the airframe. So for the BO 105 helicopter, e.g., the shape of the afterbody and naturally the shape of the basic fuselage influence the static and dynamic stability, as shown in Figure 2 and Reference 2.

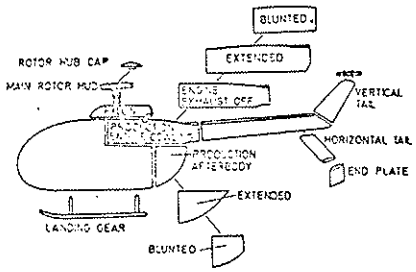

EFFECT OF / ON	TAIL EFFEC-TIVENESS	STABI-LITY	V_{CRUISE}
BASIC FUSELAGE	F	P P P	P P F
AFTERBODY	S S S	S S S	S S
ENGINE COWLING	S	S S	S
P Y L O N	S S	S	P S
MAIN ROTOR HUB	S S	S	P S
LANDING GEAR			P S
TAIL BOOM		P	P F
TAIL & ENDPLATES		P P P	P P
TAIL ROTOR HUB			P

INFLUENCE [XXX] GREAT [ ] SMALL
VIA [P] PRESSURE [F] FRICTION [S] SEPARATION

Figure 2 Influence of Airframe Components on Performance of a Typical Utility Helicopter

At given non-aerodynamic requirements, a helicopter airframe designer should try to

- avoid separation to get low pressure drag and good stability,
- minimize the wetted area for low skin friction drag,
- avoid negative lift (and the associated induced drag) at cruising conditions,
- minimize wake/tail interference for good tail effectiveness and stability.

In terms of airframe components the designer preferably has to optimize

- the basic fuselage concerning drag and stability due to pressure and skin friction,
- the afterbody, the rotor hub and pylon and the engine cowling concerning drag and stability due to separation and wake/tail interference,
- the landing gear concerning drag,
- the tail unit to have good stability.

Expensive wind tunnel tests necessary to do this job may be reduced using an analytical model to calculate the viscous flow around helicopter bodies including separation effects.

2. Analytical Model

2.1 Objectives and State of the Art

Meeting the helicopter designer's need, an analytical method should be able to calculate

- velocities and pressure around body and tail,
- skin friction around the fuselage,
- separated flow around some parts of the body,
- velocities and pressure in the wake,
- wake-tail interference,
- rotor-body-tail interferences

in consideration of

- helicopter roll/yaw/pitch angle,
- free stream velocity,
- rotor geometry and disk loading.

Neglecting skin friction and separated flow, velocities and pressure can be calculated around arbitrary configurations using potential flow panel methods well known from fixed wing application, e.g. References 3 and 4. Skin friction and separation areas may be estimated by boundary layer calculation procedures. Since three-dimensional boundary layer techniques are not fully established for engineering purpose particularly with regard to three-dimensional separation, quasi-two-dimensional boundary layer techniques can be used following the small cross-flow assumption, References 5 and 6. To simulate separation areas, source panels can be used to inject fluid, see Reference 7. Although this method yields much improved surface pressure distributions ahead of separated regions, it cannot simulate the pressure and velocities inside the wake to calculate wake-tail interference.

Using powerful potential flow panel methods, quasi-two-dimensional boundary layer techniques and a new wake concept in the separated flow areas (Reference 8), it should be possible to meet most of those objectives, mentioned above. The result should be an analytical technique for fuselage design and optimisation useful for preliminary design studies of new helicopters.

2.2 Potential Flow Model for Inviscid Flow

Taking advantage of experiences with fixed wing body aerodynamics (Reference 4), a source type panel method for three-dimensional flow around arbitrary body configurations has been adopted: Velocity $\vec{u}(x, y, z)$ of the flow is calculated by summing up the free stream velocity $\vec{u}_\infty$ and the velocity $\vec{u}_\sigma$ induced from source covered surface s of the body:

$$\vec{u}(x, y, z) = \vec{u}_\infty + \vec{u}_\sigma(x, y, z). \qquad (1)$$

Source induced velocity u_{σ_p} at a point of reference p is

$$\vec{u}_{\sigma_p} = -\frac{1}{4\Pi} \nabla \iint_{(s)} \frac{\sigma(s)}{r(s, p)} \, ds \qquad (2)$$

where $\sigma_{(s)}$ and r(s, p) are the source distribution at s and the distance from s to p.

Using the boundary conditions

$$\vec{u}(x, y, z) = \vec{u}_\infty \text{ for } x, y, z \to \infty \qquad (3)$$

and

$$u_{\sigma_n} = -\vec{n} \cdot \vec{u}_\infty \text{ at s}$$

(where $\vec{n}$ and u_{σ_n} are the normal vector and normal component of source induced velocity) the well known integral equation

$$\frac{\vec{n}}{4\Pi u_\infty} \cdot \nabla \iint_{(s)} \frac{\sigma(s)}{r\,(s, p)} \, ds = \vec{n} \frac{\vec{u}_\infty}{u_\infty} \qquad (4)$$

for the source distribution $\sigma_{(s)}$ can be established.

2.3 Potential Flow Model for Separated Flow

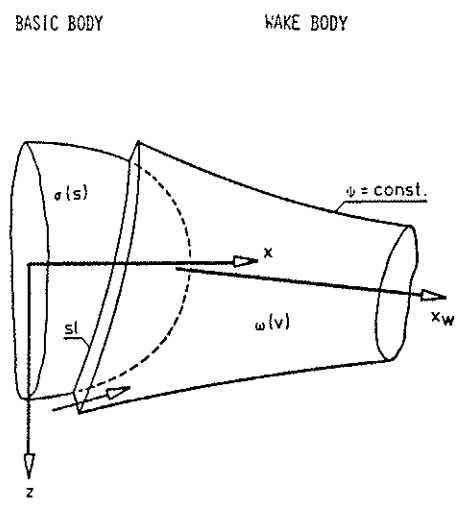

In the viscous wake behind a separated area potential flow theory is not valid. Nevertheless the effects of the vorticity can be simulated by a vortex distribution compatible with potential flow. According to Reference 4 and Figure 3 a wake body is attached to the body surface s at the separation line sl. The wake body's volume v has a vorticity distribution ω(v).

Figure 3 Potential Flow Model for Separated Viscous Flow around 3-Dimensional-Bodies

The velocity at any point then is

$$\vec{u}(x, y, z) = \vec{u}_\infty + \vec{u}_\sigma(x, y, z) + \vec{u}_\omega(x, y, z) \qquad (5)$$

where the vortex induced velocitiy $\vec{u}_\omega$ at a point p is

$$\vec{u}_{\omega_p} = -\frac{1}{4\Pi} \iiint_{(v)} \omega(v) \frac{\vec{e}_\omega x \vec{r}(v,p)}{[r(v, p)]^3} dv \qquad (6)$$

and $\vec{e}_\omega$ is the unity vector of the vorticity ω.

Additional boundary conditions have to be met:
At the wake surface the stream function ψ is constant and the vorticity vanishes:

$$\left.\begin{aligned} \omega\ (v) &= 0 \\ \psi(x, y, z) &= \text{constant} \end{aligned}\right\} \quad \text{at wake surface.} \qquad (7)$$

At the separation line sl the shear stress τ_{sl} of the boundary layer vanishes and a vorticity $(\partial\omega/\partial x_w)_{sl}$ is spread from the boundary layer into the wake. The vorticity distribution along the wake coordinate x_w may be governed by.

$$\frac{\partial \omega}{\partial x_w} = \frac{\partial \omega}{\partial x_w}\Big|_{sl} \cdot f\ (x_w) \qquad (8)$$

where f (x_w) is a function to be defined later.

Following the equations (5, 6) and the boundary conditions (7, 8), the integral equation (4) changes to

$$\frac{\vec{n}}{4\Pi u_\infty} \left[\nabla \iint_{(s)} \frac{\sigma(s)}{r(s, p)} ds + \iiint_{(v)} \omega(v) \frac{\vec{e}_\omega \times \vec{r}(v,p)}{[r(v, p)]^3} dv\right] = \vec{n} \cdot \frac{\vec{u}_\infty}{u_\infty} \qquad (9)$$

which is nonlinear for σ (s), because of the dependence of ω (v) on σ(s) via the boundary conditions.

To solve equation (9), an iterative solution technique is given below.

3. Numerical Solution

3.1 Discretisation of Body and Wake

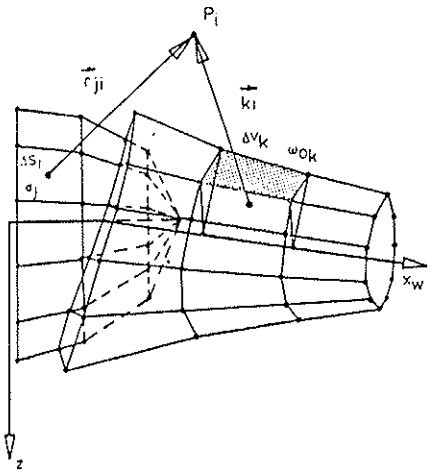

Figure 4 Discretisation of Body and Wake

Numerical solution of equation (9) is obtained by a panel technique: The body surface is divided into suitable quadrilaterals Δs covered with a source distribution of constant strength σ, and the wake is divided into triangular prismatic volume elements Δv with a continuous vorticity distribution of the strength $\omega_o(v)$, see Figure 4. So the integral equation (9) is decomposed into a nonlinear summation equation

$$\frac{\vec{n}}{4\pi u_\infty} \cdot \nabla \sum_{(s)} \frac{\sigma}{r} \cdot \Delta s = \vec{n} \frac{\vec{u}_\infty}{u_\infty} - \frac{\vec{n}}{4\pi u_\infty} \sum_{(v)} \frac{\omega_o}{r^3} \cdot \Delta v \; . \qquad (10)$$

Since a given vortex distribution ω makes the system of equations (10) linear, the problem may be formulated as an iterative resolvable nonlinear system

$$[A_{ij}] \quad \{ x_i \} = \{ B_i \} \qquad (11)$$

where the coefficient matrix is

$$A_{ij} = \vec{n}_i \cdot \vec{C}_{ij} \qquad (12)$$

with the influence coefficient C_{ij} of the surface element number j on the point number i. The vector of unknown surface singularities is

$$x_i = \sigma_i \frac{1}{4\pi u_\infty} \qquad (13)$$

and the right hand side vector is

$$B_i = -\vec{n}_i \cdot \frac{\vec{u}_\infty}{u_\infty} + \vec{n} \sum_k \omega_{ok} \vec{D}_{ik} \qquad (14)$$

with the influence coefficient D_{ik} of the wake element number k on the point number i.

To solve equation (11) the following iteration method is convenient (starting with $\omega_{ok} = 0$):

- calculation of σ_j by solving the linear system (11),
- calculation of D_{ik} and ω_{ok} from boundary conditions equations (7, 8),
- repetition of these steps until convergence is achieved,
- calculation of velocities from equation (5).

3.2 Calculation of Influence Coefficients C_{ij}, D_{ik}

The source distribution σ_j is constant over each surface element Δs_i. Therefore the influence coefficients C_{ij} of a surface element number j on a point number i can be calculated by

$$\vec{C}_{ij} = \nabla \iint_{\Delta s_j} \frac{ds}{r_{ij}} , \qquad (15)$$

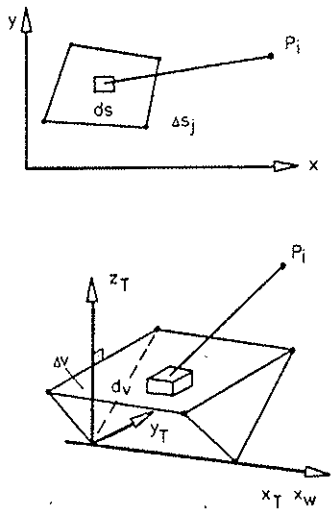

see Figure 5. For the numerical integration procedure and its simplifications in case of r_{ij} becoming large compared to the element's diameter see Reference 3.

Figure 5 Calculation of Influence Coefficients C_{ij}, D_{ik}

The vorticity distribution $\omega(v)$ is continuous and may be described by

$$\omega(z_T, x_T) = \omega_o(x_T) \cdot \bar{\omega}\ (z_T) \qquad (16)$$

where x_T and z_T are wake element coordinates, see Figure 5. The influence coefficients D_{ik} of a wake element number k on a point number i can be calculated by

$$\vec{D}_{ik} = \iiint_{\Delta V_k} \bar{\omega}\ (z_T) \cdot \frac{\vec{e}_{y_T} \times \vec{r}_{ki}}{r_{ki}^3}\, dv. \qquad (17)$$

Numerical details of the integration and its simplifications can be found in Reference 8.

3.3 Calculation of Wake Geometry

Wake geometry (Figure 6) is governed by the boundary condition equations.

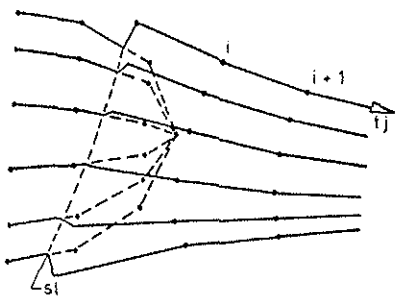

Figure 6 Calculation of Wake Geometry

The beginning of the wake, that is the separation line, is obtained by boundary layer calculation. This calculation is done along quasi two-dimensional bodies of revolution, calculated for each surface streamline. Streamlines are calculated by a two-dimensional spline interpolation for surface geometry and velocities, Reference 6.

At the separation line (index sl) the surface streamlines are shifted to a position that is a distance δ_{sl} above the body surface, where δ_{sl} is the boundary layer thickness at the separation line. At these points a calculation procedure for free streamlines is established, which form the convex surface of the wake.

Streamline calculation at the body as well as the wake surface is done using the influence coefficients C_{ij} and D_{ik} defined in equations (15, 17) for any point number i in space.

3.4 Calculation of Wake Vorticity

From two-dimensional potential theory the vorticity (rotation) is known to be

$$\omega = \frac{\partial u}{\partial z} - \frac{\partial w}{\partial x} \qquad (18)$$

with the velocity components u, w in any rectangular system x, z. According to the empirical velocity distribution at some stations in the wake shown in Figure 7 local vorticity distributions shown may be used to generate those velocity distributions. The vorticity distributions may be represented by

$$\omega(z_T,\ x_T) = \omega_o(x_T) \cdot \bar{\omega}(z_T) = \qquad (19)$$

$$= \omega_o(x_T) \cdot [a_1 + a_2(z_T - z_{1T}) \ \ldots\ + a_4(z_T - z_{1T})^3]$$

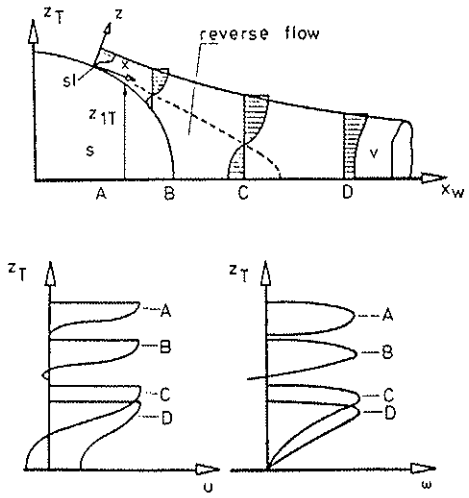

Figure 7 Calculation of Wake Vorticity

The constants a_1 to a_4 in equation (19) depend on x_T and may be determined at some points, e.g. at separation line and at a position far off the body assuming a linear behaviour between these points.

Integrating equation (18) at separation line across the boundary layer thickness δ gives approximately

$$\frac{\partial \Gamma}{\partial x}\Big|_{sl} = u_{sl} \cdot c_1, \qquad (20)$$

where Γ is the vorticity ω integrated over z.
The vorticity distribution along the wake coordinate x_w may be described by

$$\frac{\partial \Gamma}{\partial x_w} = \frac{\partial \Gamma}{\partial x_w}\Big|_{sl} \sqrt{\frac{a}{a_{sl}}} \cdot e^{-c_2 \cdot x_w}, \qquad (21)$$

where a is the cross section area of the wake. The damping factors c_1 and c_2 will be adjusted using emperical results.

3.5 Iterative Computation Outline

The iterative calculation procedure to solve the nonlinear system of equations (11) is shown in Figure 8:

- First a discretization program generates the panel geometry of the body using the body surface nodalpoints as input data.
- As a second step the potential flow equation for the panel configuration is solved, neglecting wake influence when running the first iteration loop. Velocities and singularities on body surface are the result.
- Thirdly streamline calculation is started using body surface nodalpoints and velocities as input data. The

result is the streamline geometry and velocity profile on body surface.

- The fourth step consists of the quasi-two-dimensional boundary layer calculation leading to the separation line on the body surface.
- The final step is the wake calculation and provides the wake geometry and vorticity using the surface and wake singularities and the separation line data as input.
- At this point the next iteration loop is started solving again the potential flow equation (see second step) including the influence of the wake.

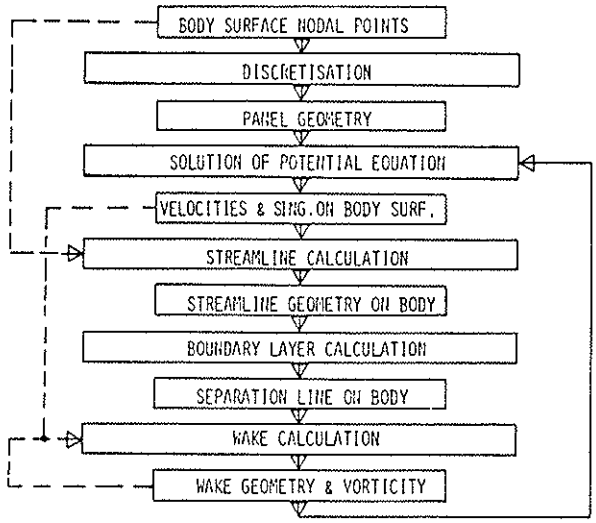

Figure 8 Iterative Solution Scheme

4. Results and Discussion

4.1 Separated Viscous Flow around a Sphere

The vorticity generation factor c_1 and the vorticity decay factor c_2, defined in 3.4, have to be adjusted using empirical results. c_1 represents the ratio between the vorticity in the wake and the vorticity generated by the boundary layer at the separation line. c_2 forces the vorticity in the wake to decrease along the wake coordinate x_w according to equation (21).

Parametric investigations have been made calculating the separated viscous flow around a sphere. An example is shown in Figure 9. The factor c_1 which primarily influences the wake diameter is set equal to unity and the factor c_2 which mainly influences the length of reversed flow region is chosen to be 0.5.

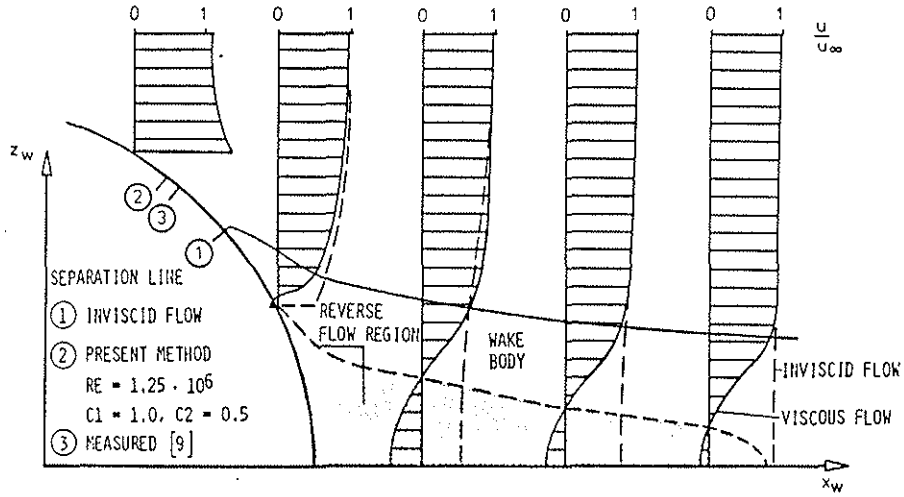

Figure 9 Separated Flow around a Sphere

Unfortunately flow field measurements were not available exept velocity profiles at a position far downstream. The calculated flow field shows typical viscous separation effects: Boundary layer separation line is shifted upstream compared to inviscid calculation and agrees well with measurements (Reference 9). The reverse flow region vanishes at a distance of about one diameter downstream from the sphere. Though this might be a rather long distance, a better adjustment by c_2 could not be made because of the lack of suitable flow field measurements. But the difference between the velocity profiles in the wake according to inviscid and separated potential flow theory proves that velocities in the wake (e.g. for wake-tail interferences) can only be calculated correctly by using a separated flow model such as the one described above.

4.2 Flow Field around a Helicopter Body

The arrangement of 640 panels used to calculate the viscous flow around the BO-105 fuselage is shown in Figure 10. Typical results for angles of attack between -10 and 10 deg. and RE/meter = 1.4×10^6 1/m corresponding to a wind tunnel test (Reference 10) of a 1:4 model at 150 kts can be seen in Figure 11. Side views of the streamlines around the body and of the wake geometry are given.

The separation line is fixed behind the rotor pylon whereas the size of the separation area behind the afterbody varies according to the angle of attack. Therefore the helicopter stability is influenced by the changing pitching moment. On the production fuselage of BO-105 the separation line at the afterbody is fixed by a spoiler to avoid this destabilizing effect.

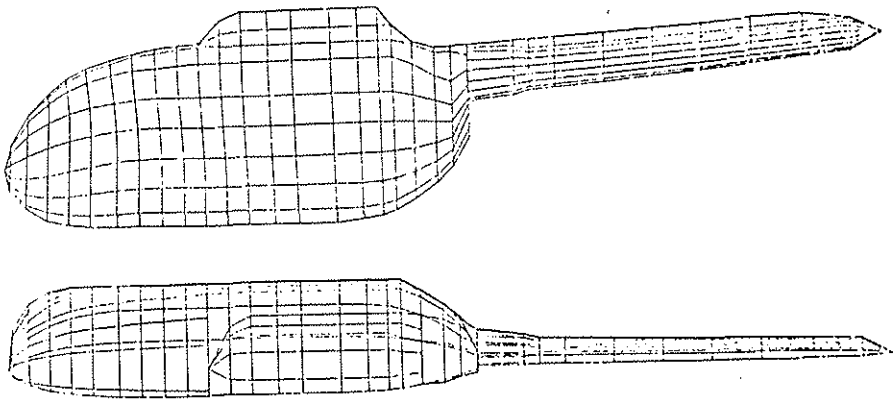

Figure 10 Panelarrangement of BO-105 Fuselage

According to Figure 11 the influence of the wake on the tail schould be small at cruising conditions i.e. α = -5 to 10 deg. But the wake of the rotor hub, which is not included in this calculation, can be expected to influence the tail and tail-rotor following the wake streamlines calculated for the pylon.

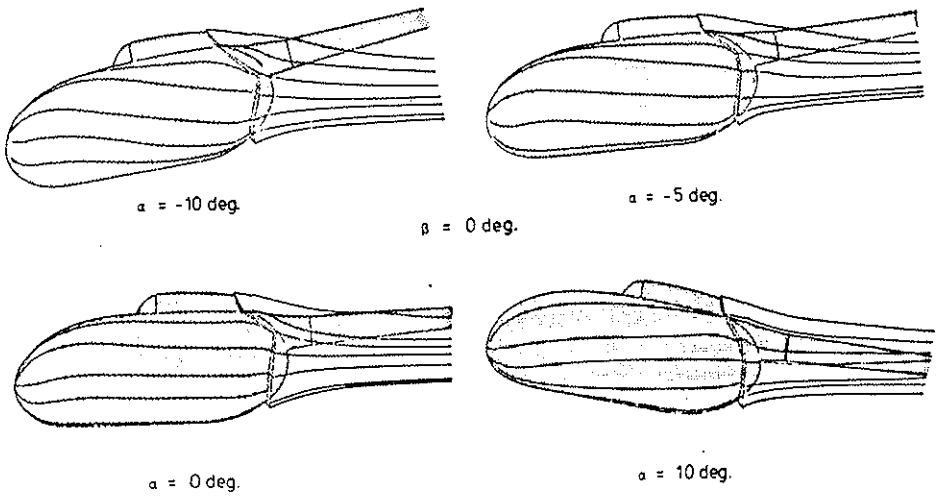

Figure 11 Separated Flow around BO-105 Body Streamlines and Wake

For the flow fields around the BO-105 fuselage shown in Figure 11 a comparison of measured and calculated separation lines is presented in Figure 12. The separation lines neglecting separated flow effects are also shown. These are the results from the first iteration loop of the procedure.

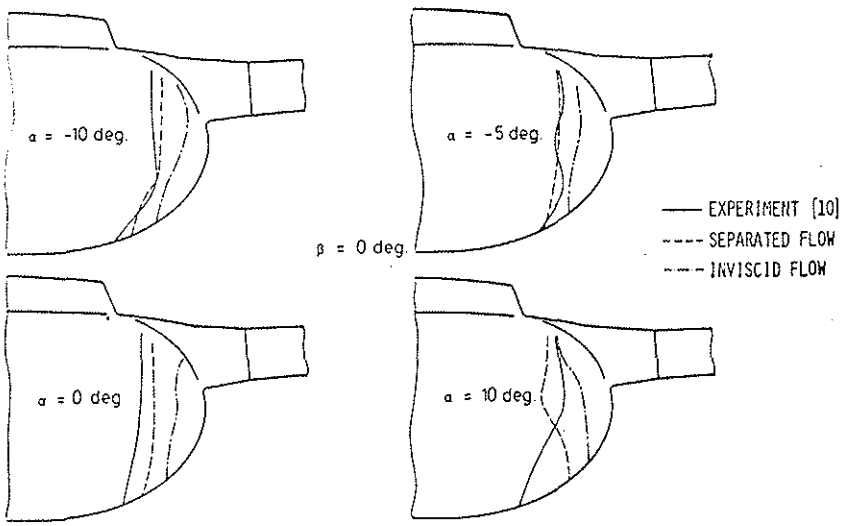

Figure 12 Separated Flow around BO-105 Body Comparison with Experiment

Experimental separation lines in the cruise speed angle of attack regime, i.e. $\alpha = -5$ to -10 deg., agree very well with the separation lines calculated under consideration of separation effects. In the angle of attack regime of $\alpha = 0$ to 10 deg. the agreement is not as good, but the results including separation effects are generally better than those neglecting them.

5. Conclusions

An analytical technique that takes into account essential separation effects in the design of new helicopter fuselages has been presented in this paper:

Potential flow panel methods well known from fixed wing application can be used to calculate inviscid flow around arbitrary three-dimensional configurations. Quasi-two-dimensional boundary layer techniques are able to estimate skin friction and separation lines. Separation effects can be simulated by a vortex body attached to the basic body at the separation area.

A nonlinear integral equation for the singularities at the body surface and in the wake is given. Solution is done by discretisation followed by an iterative calculation procedure starting with inviscid potential flow.

Results are the velocities of the flow field around the body, in the separated flow region, and in the wake. They can be used to calculate forces and moments acting on the fuselage and to calculate wake-tail-interferences.
Results for the separated flow around a sphere and a helicopter fuselage show the effectiveness of the method in calculating the separated flow area, the separation wake geometry, and the velocity field in the wake.

Further developments of the method should include rotor downwash effects to handle rotor-body-tail-tailrotor interferences.

6. References

1. S.N. Wagner, Problems of estimating the drag of a helicopter, AGARD Conference On Aerodynamic Drag, April (1973)

2. C.N. Keys and W.L. Ballauer, Analysis of the BO-105 drag and stability investigation wind-tunnel-tests, Boeing Vertol Rep. No. D212-10021-1, (1970)

3. J.L. Hess and A.M.O. Smith, Calculation of nonlifting potential flow about arbitrary three-dimensional bodies, McDonnell-Douglas Report ES 40622, (1962)

4. W. Kraus and P.Sacher, Das MBB-Unterschall-Panel Verfahren:
   Teil I: Das Verdrängungsproblem ohne Auftrieb in kompressibler Strömung, MBB Report UFE 632-70 (1970)
   Teil II: Das auftriebsbehaftete Verdrängungsproblem in kompressibler Strömung, MBB Report UFE 633-70 (1970)
   Teil III: Flügel-Rumpf-Kombination in kompressibler Strömung, MBB Report UFE 634-70 (1970)

5. F.R. De Jarnette, Calculation of inviscid surface streamlines and heat transfer on shuttle type configurations, NASA CR-111921 (1971)

6. R. Stricker, W. Gradl, and G. Polz, Aerodynamische Arbeitsgrundlagen für zukünftige Hubschrauberentwicklungen, MBB Report No. UD-159-75 (1975)

7. F.A. Woodward, F.A. Dvorak and E.N. Geller, A computer program for three-dimensional lifting bodies in subsonic inviscid flow, USAAMRDL-TR-74-18 (1974)

8. R. Stricker, W. Gradl and G. Polz, Aerodynamische Grundlagen für zukünftige Hubschrauberentwicklungen, MBB Report No. UD-194-6 (1977)

9. O. Flachsbarth, Drag characteristics of spheres with and without turbulence, Physik.Zeitschr. 1927 p. 461 (1927)

10. J. Gillespie and R.I. Windsor, An experimental and analytical investigation of the potential flow field, boundary layer, and drag of various helicopter fuselage configurations, USAAMRDL Tech.Note 13, Ft.Eustis, Va. Jan (1974)